Reshaping Dynamics of Gold Nanoparticles under H2 and O2 at Atmospheric Pressure

Adrian Chmielewski, Jun Meng, Beien Zhu, Yi Gao, Hazar Guesmi, Hélène Prunier, Damien Alloyeau, Guillaume Wang, Catherine Louis, Laurent Delannoy, et al.

Reshaping Dynamics of Gold Nanoparticles under H_2 and O_2 at Atmospheric Pressure

Adrian Chmielewski,[†] Jun Meng,[‡,¶,§] Beien Zhu,[‡] Yi Gao,[‡] Hazar Guesmi,[§] Hélène Prunier,[†] Damien Alloyeau,[†] Guillaume Wang,[†] Catherine Louis,[‖] Laurent Delannoy,[‖] Pavel Afanasiev,[⊥] Christian Ricolleau,[†] and Jaysen Nelayah[*,†]

†*Université Paris Diderot, Sorbonne Paris Cité, CNRS, Laboratoire Matériaux et Phénomènes Quantiques, UMR 7162, 75013, Paris, France.*

‡*Division of Interfacial Water and Key Laboratory of Interfacial Physics and Technology, Shanghai Institute of Applied Physics, Chinese Academy of Sciences, Shanghai 201800, China.*

¶*University of Chinese Academy of Sciences, Beijing 100049, China.*

§*Institut Charles Gerhardt Montpellier, CNRS/ENSCM/UM, 240, Avenue du Professeur Emile Jeanbrau, 34090 Montpellier, France.*

‖*Sorbonne Université, UPMC Univ Paris 06, UMR CNRS 7197, Laboratoire de Réactivité de Surface, 4 Place Jussieu, Tour 43-33, 3éme étage, Case 178, F-75252 Paris, France.*

⊥*Univ Lyon, Université Claude Bernard - Lyon 1, CNRS, IRCELYON - UMR 5256, 2 Avenue Albert Einstein F-69626 Villeurebanne cedex, France.*

E-mail: jaysen.nelayah@univ-paris-diderot.fr

Phone: +33 (0)1 57 27 69 98. Fax: +33 (0)1 57 27 62 41

Abstract

Despite intensive research efforts, the nature of the active sites for O_2 and H_2 adsorption/dissociation by supported gold nanoparticles (NPs) is still an unresolved issue

in heterogeneous catalysis. This stems from the absence of a clear picture of the evolution of the structural properties of Au NPs in the presence of these gases at near reaction conditions, i.e. at high pressures and high temperatures. We hereby report on the first real-space observation of the equilibrium shapes of TiO_2-supported model Au NPs under O_2 and H_2 at atmospheric pressure using window gas cell transmission electron microscopy (GCTEM). *In situ* GCTEM observations show instantaneous changes in the equilibrium shape of Au NPs under O_2 during cooling from 400 °C to room temperature. In comparison, no instant change in equilibrium shape is observed under H_2 environment. To interpret these experimental observations, the equilibrium shape of Au NPs under O_2, atomic oxygen and H_2 gas environments was predicted using a multiscale structure reconstruction model. Excellent agreement between GCTEM observations and theoretical modelling under O_2 provides strong evidence for the molecular adsorption of O_2 on the Au NPs below 120 °C. Molecular adsorption takes place on specific Au facets which are identified in this work. In the case of H_2, theoretical modelling predicts weak interactions with gold atoms which explain their high morphological stability under this gas. This work provides atomic structural information for the fundamental understanding of the O_2 and H_2 adsorption properties of Au NPs under real working conditions and also shows a new way to identify the active sites of heterogeneous nanocatalysts under reaction conditions by monitoring the structure reconstruction.

Keywords

Gold nanoparticles, environmental transmission electron microscopy, H_2 adsorption, O_2 adsorption, DFT, Multi Scale structure Reconstruction model.

While bulk gold is chemically inert, gold nanoparticles (NPs) are known to be chemically reactive.[1] The unique chemical reactivity of Au at the nanoscale has since the 1970's sparked great research interests in the application of supported Au NPs as heterogeneous catalysts in the chemical industry.[2–5] The major breakthrough in gold heterogeneous catalysis occured in the 1980's following the seminal works of Haruta and collaborators on the oxidation of carbon monoxide.[6,7] Since these pioneering works, there have been numerous reports on the promotion of reactions at much lower temperatures or with much higher degrees of selectivity than over other metal catalysts using Au NPs deposited on metal oxide or carbon surfaces.[8] These reactions include, among others, the oxidation of CO mentioned beforehand,[7,9–13] the selective oxidation reactions of alcohols,[14–18] the Dussan (water-gas shift) reaction,[19] the synthesis of hydrogen peroxide[20,21] and the selective hydrogenation reactions.[22–25]

In these catalytic reactions, knowing the activation and reaction processes undergone by the reacting species is important to understand the active sites of supported Au NPs. An essential step in oxidation and reduction reactions catalyzed by supported Au NPs is the adsorption and ultimately, the dissociation of O_2 and H_2 molecules, respectively, by the metal and/or support atoms. While it has been shown that the catalytic activity of supported Au NPs depends on a number of key parameters such as temperature,[6,7] particle size and shape[24,26–28] and the contact structure of the nanoparticles with the support,[28,29] fundamental questions remain on oxidation reactions with O_2 as the oxidant and hydrogenation reactions with H_2 as the reducer. In particular, there is no general consensus on the nature of the active adsorption/dissociation sites and their localization in both types of reactions as theoretical and experimental studies undertaken on these subjects have come to conflicting conclusions, with supports found for different perspectives. For instance, in the dissociation of H_2 molecules by Au NPs supported on stoichiometric and reduced TiO_2 surfaces, density functional theory calculations predict that the active sites are the low-coordinated neutral gold atoms located at corner or edge sites with no direct bonding to the support.[30,31] The dissociative adsorption of hydrogen limited to Au atoms at corner and edges positions was

also suggested following experimental studies of Au/Al_2O_3 catalysts using a combination of *in situ* X-ray absorption spectroscopy, chemisorption, and hydrogen-deuterium exchange experiments.[32] In contrast, other experimental works report that the perimeter of the interface between gold NPs and their supports are the active sites for hydrogen dissociation.[33,34] Similarly, in the interaction of supported Au NPs with O_2, both low-coordinated Au atoms located at corner or edge positions[9,35,36] and metal-support sites at the perimeter[37–40] are proposed as active sites for the adsorption and dissociation of O_2 molecules. The absence of a consensus on these issues is due to the lack of a clear picture of the evolution of the structural properties of Au NPs under O_2 and H_2 at near reactions conditions, i.e. at high pressures and high temperatures.

In this work, we provide the first real-space snapshots of the morphological dynamics of titania-supported model Au NPs under O_2 and H_2 at atmospheric pressure using window gas cell environmental transmission electron microscopy (GCTEM). It has been experimentally observed and theoretically predicted that the bonding between the NP and the reactant could induce dynamic morphology changes of the NPs.[41–43] By combining real-time *in situ* environmental TEM observations of particle equilibrium shape (ES) of Au NPs under gas atmospheres and multi-scale structure reconstruction (MSR) modeling, we additionally provide valuable atomic level insights on Au surface reconstruction induced by the adsorptions of O_2 and H_2 molecules. The dynamic shape changes under O_2 observed experimentally and predicted by MSR identify that the Au low-coordinated atoms can instantly and directly bind O_2 molecules at room temperatures. Under H_2, no instant shape change is observed, indicating a weak interaction between Au NPs and H_2 molecule.

For a better understanding of the reactivity of gold and gold-based nanocatalysts, a number of environmental microscopies have been used to study *in situ* the structural parameters under reactive gas environments over a wide range of pressure and temperature.[44,45] Among these microscopies, environmental gas transmission electron microscopy has emerged as an important tool enabling real-time atomic-scale visualization of structural evolutions of

nanomaterials under gas environments and temperature.[46–52] It has already provided some insights into the reactivity of Au NPs with O_2 and H_2 molecules through atomic-scale and real-time visualization of particle ES under these gases.[48,53,54] However, environmental gas TEM observations of Au NPs under O_2 and H_2 have until now been limited to low pressure conditions of little relevance to catalytic reactions. The present works ambitions to bridge this pressure gap in the study of Au NP under O_2 and H_2. Moreover, despite the successful use of MRS model in other systems, it is also the first time that the equilibrium structure of Au NP under high O_2 and H_2 pressure is modeled and analyzed theoretically.

In situ monitoring of the ES of supported Au NPs under O_2 and H_2 atmospheres were carried out using chemically-sensitive high-angle annular dark field (HAADF-STEM) imaging on a JEOL JEM-ARM200F microscope operated in scanning transmission electron microscopy (STEM) mode. The gaseous media were confined in a restricted zone around the sample in the TEM using an environmental high temperature and high pressure gas cell (HTPGC) from Protochips Inc. The gas cell is a modified version of the Atmosphere TEM environmental gas cell from the same company. It incorporates two microfabricated silicon chips (so called E-chips). It can withstand static and dynamic gas environments up to atmospheric pressure and temperatures up to 1200 °C. Figure 1a shows a low magnification scanning electron microscopy image of the E-chip which serves both as particle support and heater. It is patterned with six electron transparent SiN windows for TEM observation. Surfactant-free Au NPs were synthesized by pulsed laser deposition (PLD) in a high vacuum chamber at 10^{-5} Pa. Au NPs were deposited on rutile titania (r-TiO_2) nanorods synthesized by hydrothermal method and exposing (110) facets.[55] TiO_2 is a good metal oxide support for Au NPs due to its strong interaction with the latter and its chemical stability among others.[56] The (110) facet is the most stable facet of r-TiO_2 and is widely used as substrate in heterogeneous catalysis.[57] The nanorods were deposited prior to metal deposition on the smaller heater E-chip of the HTPGC. The low magnification (×1M) HAADF-STEM image in Figure 1b shows r-TiO_2 nanorods randomly dispersed on one of the SiN windows. The

nanorods were heated at 300 °C during metal deposition and the nominal thickness of metal deposited fixed to 1 nm to obtain NPs with a mean particle in-plane size around 5 nm, a size range where TiO_2-supported Au NPs in fact start to be active.[33,58] Further experimental details on electron microscopy, the gas cell and sample preparation are provided in the Supporting Information. Besides O_2 and H_2, Au NPs were also studied *in situ* under residual argon gas in a benchmark experiment.

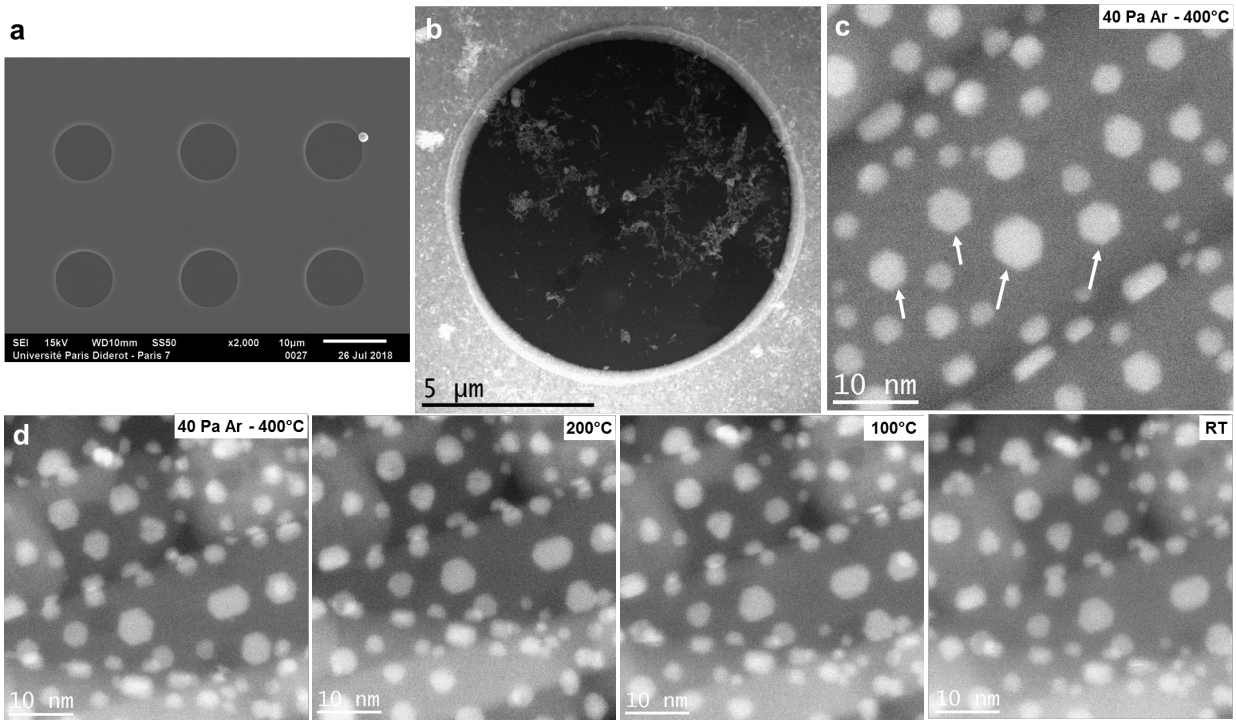

Figure 1: **Sample preparation for GCTEM and *in situ* GCTEM observation of Au NPs supported on r-TiO_2 nanorods exposing (110) surfaces under inert Ar atmosphere**. (a) SEM image of the E-chip used both as sample support and heater in the Protochips gas cell. The scale bar indicates 10 µm. There are six 9 µm large windows overlaid with an electron transparent SiN film. TEM observations are carried out at these windows. (b) HAADF-STEM image showing a random deposition of r-TiO_2 nanorods on one of the SiN windows. (c) HAADF-STEM image of Au NPs deposited by pulsed laser deposition on the r-TiO_2 nanorods and exposed to 40 Pa of Ar at 400 °C. Indexation of the projected outlines of the NPs in the HAADF-STEM image indicates that they have a truncated ES bounded by major {111} and {100} facets of the Au fcc structure. Some truncated octahedra imaged closed to the [101] zone axis are indicated by white arrows. (d) Temperature series of HAADF-STEM images of another assembly of TiO_2-supported Au NPs cooled from 400 °C to room temperature under 40 Pa Ar. The particle size distribution and the truncated octahedron ES of the NPs are stable with temperature.

Under all gases, the Au NPs were first heated *in situ* to 400 °C and their ES were imaged at different temperature steps while cooling the samples to RT. Figure 1c shows a higher magnification (×5M) HAADF-STEM image of an assembly of Au NPs on the r-TiO_2 support under 40 Pa Ar after *in situ* heating to 400 °C. The in-plane particle size measured from the HAADF-STEM image is below 6 nm. By measuring the projection angles between the edges of the projected outlines of individual NPs and comparing them with the angles between crystal planes of the Au fcc structure with different Miller Indices (see Figure S1 in supplementary information), we deduce that the particle outlines are bounded mainly by {111} and {100} edge-on facets pointing to a nearly truncated octahedron ES as observed in similar Au NPs under vacuum.[59] In Figure 1c, the majority of the truncated octahedra are viewed close to the [101] zone axis (like the ones pointed by white arrows). Along this direction, their STEM projection images display a 3-fold symmetry. The anisotropy ratio $\gamma_{100}/\gamma_{111}$ between the surface energies of the {100} and {111} facets, determined by applying Wulff construction to the projected HAADF-STEM images of 5 NPs in [101] zone axis, is 1.10 ± 0.04. In comparison, the $\gamma_{100}/\gamma_{111}$ ratio determined in vacuum for TiO_2-supported Au truncated octahedra is 1.08 ± 0.04 (Figure S2). Thus, at 400 °C under Ar gas, the Au NPs adopt a vacuum Wulff-Kaishev ES.

To establish the temperature dependence of the ES, we have studied an assembly of TiO_2-supported Au NPs cooled under 40 Pa Ar in a stepwise manner from 400 °C to RT with 100 °C temperature increments at a cooling rate of 1 °C/s between two consecutive steps. This cooling rate is applied in all cooling experiments presented afterhand in this work. Figure 1d shows the corresponding temperature series of HAADF-STEM images of the NPs. Here, the NPs are supported on both r-TiO_2 nanorods and anatase TiO_2 NPs. The anatase nanostructures are produced as residual by-products during the synthesis of rutile nanorods. Analysis of the projected HAADF-STEM images of individual NPs on r-TiO_2 shows NPs oriented close to the [101] zone axis as well as in other zone axes along which their projected images show no particular symmetry. During the cooling process, we first observe that, due

to the strong interactions between the TiO_2 supports and the Au NPs, the latter do not diffuse on the supports leading to a stable size distribution with temperature. Secondly, the NPs keep their truncated octahedron ES down to RT. This benchmark experiment shows that in the absence of an interaction between the Au NPs and its gas environment, the ES, below 400 °C, is of Wulff-Kaishev type with $\gamma_{100}/\gamma_{111}$ ratio equal to about 1.10. ES is driven solely by the sample temperature and particle-support interaction. Following this observation, we have performed *in situ* GCTEM studies of the evolution of ES of the Au NPs under O_2 and H_2 at atmospheric pressure and below 400 °C to unveil the interaction of the Au NPs with these molecules.

Figures 2a-d show a temperature series of HAADF-STEM images of Au NPs on r-TiO_2 nanorods acquired just after the temperature has been set successively at 400 °C, 200 °C, 100 °C and RT under 10^5 Pa O_2. Similar to *in situ* TEM observations under Ar, the NPs display truncated octahedron ES in different zone axes at 400 °C (Figures 2a). During sample cooling, truncated octahedron ES is stable down to 200 °C (comparison of Figures 2a and b). The anisotropy ratio $\gamma_{100}/\gamma_{111}$, measured on five truncated octahedra in [101] zone axis, is equal to 1.09 ± 0.04. This clearly shows that, above 200 °C, 10^5 Pa O_2 has no effect on the ES of the particles. However, when the temperature is reduced to 100 °C or RT, we observe a rounding of particle ES (Figures 2c-d) which does not occur under Ar conditions. Particle rounding is clearly visible on the projections of those NPs initially oriented closed to the [101] zone axis which lose their 3-fold symmetry in projection. The change in particle morphology with temperature is a clear indication that the surface of the Au NPs is binding O_2 molecules. It should be noted that at each temperature step, particle ES is stabilized instantaneously and it does not evolve until the temperature is reduced to the following step. Moreover, a similar rounding of particle shape is observed upon cooling under O_2 at lower pressure (133 Pa O_2, see Figure S2 in supplementary information).

In order to gain more detailed information of the observed morphological transformation in Figures 2c-d, we have followed the change in the projected ES of individual Au NPs

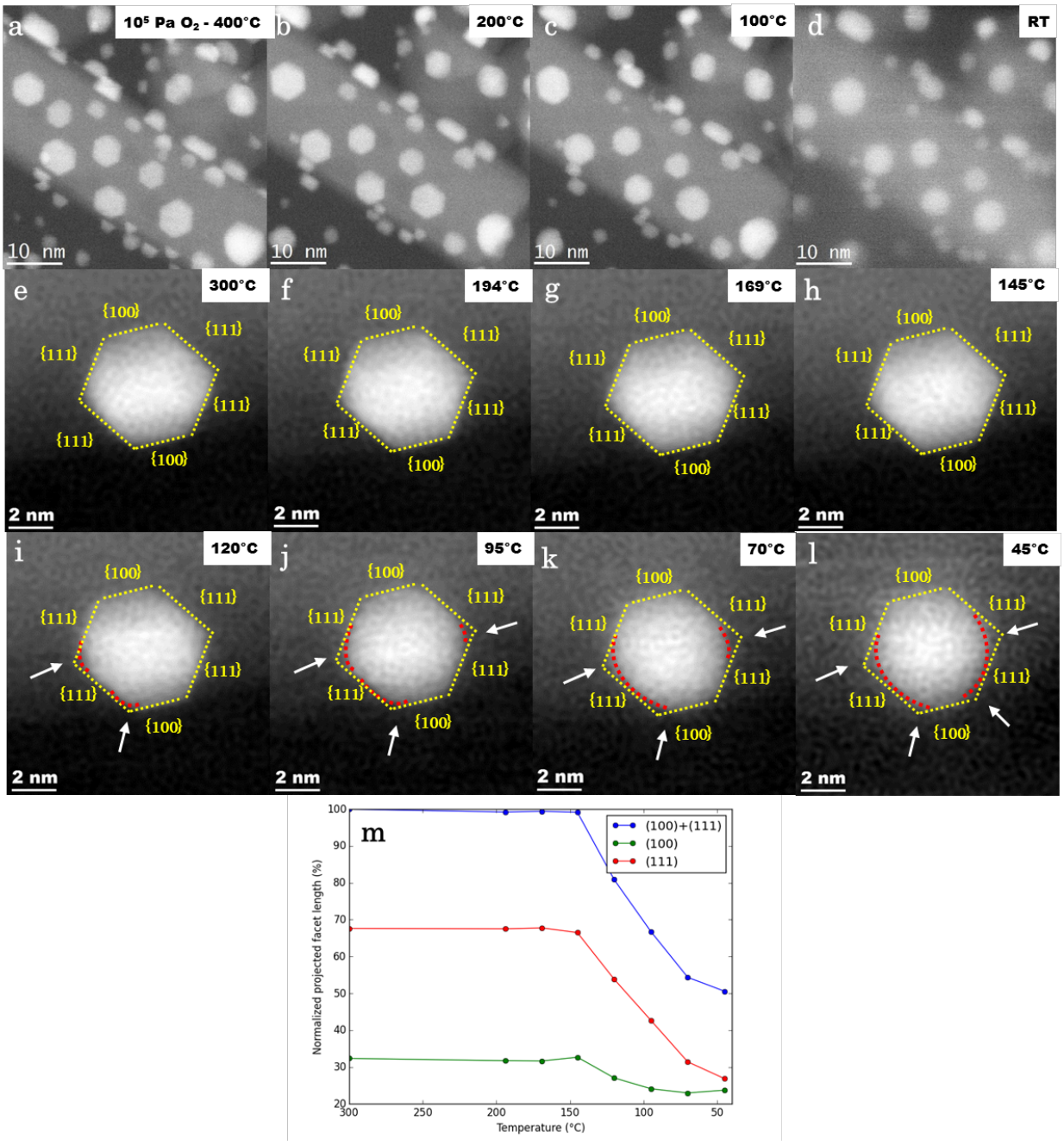

Figure 2: ***In situ* HAADF-STEM observation of Au NPs on r-TiO_2(110) surfaces under O_2 at atmospheric pressure**. Temperature series of HAADF-STEM images of TiO_2-supported Au NPs during cooling under 10^5 Pa O_2 at (a) 400 °C, (b) 200 °C, (c) 100 °C and (d) RT. Unlike under Ar in Figure 1, particle ES evolves with temperature with the particle morphology becoming rounded at low temperature. (e)-(l) Temperature series of HAADF-STEM images over the temperature window where the octahedron-to-round morphology transition is observed. The temperature onset for this transition is situated at about 120 °C. (m) Quantitative follow-up of the extension of the {111}- and {100}-type segments delimiting the particle outline in projection as a function of temperature.

viewed close to [101] zone axis between 200 to 45 °C using HAADF-STEM imaging at ×10M magnification, as shown in Figures 2f-l. For comparison, the HAADF-STEM image of the NP at 300 °C where it displays a perfect truncated octahedron ES is shown in Figure 2e. The particle outline at this temperature (yellow dotted lines on Figure 2e) and the Miller indices of the six edge-on facets along its perimeter are reproduced on all subsequent images in the temperature series to highlight deviations from the truncated octahedron ES during cooling. From the temperature series, we observe that the truncated octahedron ES is stable down to 145 °C (Figures 2e-h). At 120 °C, the NP outline starts to develop round edges (Figure 2i). The locations of these rounded smooth edges are indicated by white arrows and their extension delimited by red dotted lines on the corresponding STEM image. These rounded edges result from the extension of existing facets and/or stabilization of new ones between the adjacent {111} facets and between the {111} and {100} facets. These additional facets most probably correspond to the {110} facets and high-index facets such as {113} that connect {111} and {100} facets in a fcc structure.[60] Such facets possess a high density of low-coordinated atoms forming steps, edges and kinks.[61] It has been shown that these defects are catalytically active sites.[62] In comparison, the {111} and {100} facets are ordered and flat. From 120 to 45 °C, the extension of these new facets increases at the expense of the {111} and {100} ones leading to a rounded ES at 45 °C (Figures 2j-l). We also note that while particle shape changes, there is no significant variation in the size of the particle in projection.

Figure 2m shows the variation as a function of temperature of the percentage of the particle outlines in Figures 2e-l which is delimited by either {111}- (●) or {100}-type edge-on facets (●). Between 300 and 145 °C, as the ES is stable and close to a truncated octahedron, the extension of {111}- and {100}-type edge-on facets are thus constant (with the percentage of the particle outline covered by the {111} facets being equal to 67 %). As the temperature is reduced from 145 to 45 °C and the particle ES evolves with the stabilization of new facets, we observe a decrease in the extension of both the {111}- and {100}-type facets with

temperature. The rate at which the extension of the {111} facets decreases is higher than that of the {100} ones. At 45 °C, both types of edges have similar extension (equal to about 25 %). The total fraction of {111}- and {100}-type facets (•) indicates that the extension of the {111}- and {100}-type facets and the newly-developed facets are comparable at 45 °C which results in a near-perfect rounded ES in the projection at that temperature.

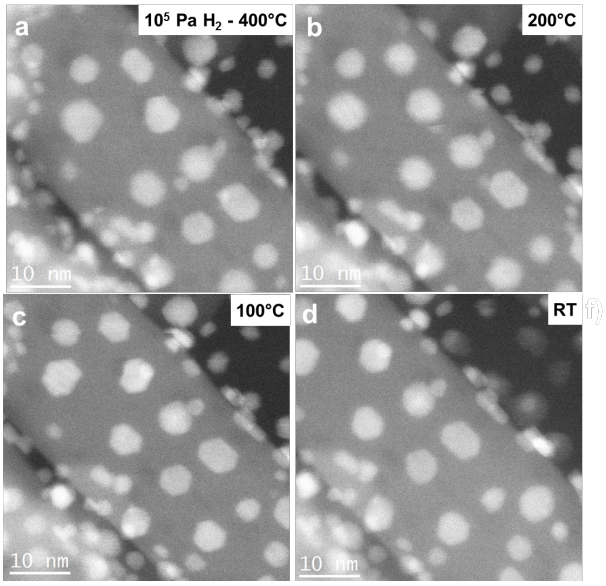

Figure 3: ***In situ* HAADF-STEM observation of Au NPs on r-TiO_2(110) surfaces under H_2 at atmospheric pressure**. Temperature series of HAADF-STEM images of TiO_2-supported Au NPs during cooling under 10^5 Pa H_2 at (a) 400 °C, (b) 200 °C, (c) 100 °C and (d) RT. As under inert Ar gas in Figure 1, particle size and their truncated octahedron ES are stable down to RT.

Figure 3 shows a temperature series of HAADF-STEM images of Au NPs on r-TiO_2 nanorods acquired under 10^5 Pa H_2 just after the temperature has been successively set at 400 °C, 200 °C, 100 °C and RT. Similar to the *in situ* observation under Ar (Figure 1), the NPs keep their initial sizes and morphologies as they are cooled to RT. The projected HAADF-STEM image of the Au NPs under H_2 are again compatible with truncated octahedron ES in different zone axes. The surface energy anisotropy ratio $\gamma_{100}/\gamma_{111}$, determined on four NPs, is equal to 1.07±0.04. This value is, within experimental errors, similar to the anisotropy ratio determined under Ar (1.10 ± 0.04).

In order to gain atomic level insights into the reshaping of Au NPs under O_2 and their high stability under H_2, we applied the multiscale structure reconstruction (MSR) model that takes into account the direct adsorption of these gases on Au NPs facets to predict the resulting equilibrium shape. This model is based on the Wulff theorem,[63] the Langmuir adsorption isotherm[64] and the density functional theory (DFT) calculations.

Under gas environments, and as detailed in previous works,[65,66] the surface tension γ_{hkl} is corrected to be the interface tension γ_{hkl}^{int} by adding the contribution of adsorbents on each (hkl) surface according to:

$$\gamma_{hkl}^{int} = \gamma_{hkl} + \theta_{hkl}\frac{E_{ads}}{A_{at}} \tag{1}$$

where θ_{hkl} is the coverage of the gas on the (hkl) facet, E_{ads} is the adsorption energy of gas molecules on this facet, and A_{at} is the corresponding area per gold surface atom.

In this equation, the coverages θ_{hkl} depend on the temperature T, the pressure P, and the value of E_{ads}. We considered the Langmuir adsorption isotherm to study the O_2@Au and the H_2@Au systems such that:

$$\theta_{hkl} = PK/(1+PK) \tag{2}$$

where K is the equilibrium constant, which can be calculated as follow:

$$K = exp(-\Delta G/RT) = exp(-E_{ads} - (S_{ads} - S_{gas})/RT) \tag{3}$$

where R is the ideal gas constant, and S_{gas} is the gas-phase entropy of the adsorbent, obtained from the NIST-JANAF thermochemical tables.[67] The S_{ads} represents the entropy in adsorbed state, which is assumed as zero. Based on the Wulff theorem, knowing the (T, P) dependent γ_{hkl}^{int} allows us to construct the ESs (equilibrium shapes) of the supported Au NP under O_2 and H_2. All energetic values of the γ_{hkl} and E_{ads}, provided in the Supporting Information (Tables S1,S2 and S3), were calculated by performing accurate DFT calculations. Three low index Au (111), (100) and (110) surfaces were considered since they represent the main facets of stable truncated octahedron nanoparticles.

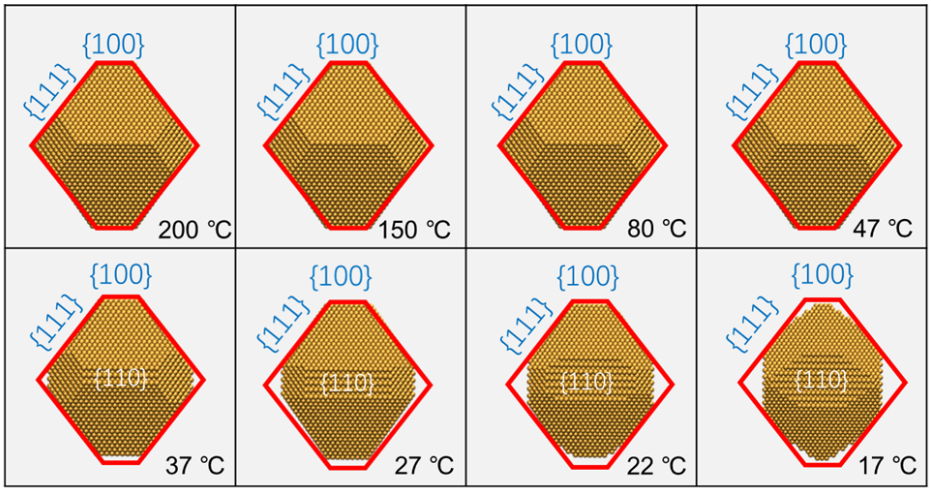

Figure 4: **Wulff construction of Au NPs under oxygen environment at atmospheric pressure as a function of temperature from 200 °C to 17 °C.**

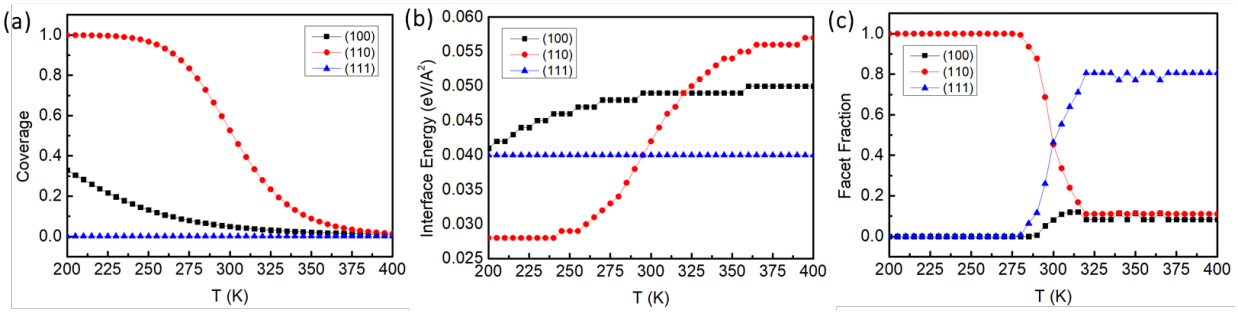

Figure 5: **(a)The coverage of oxygen molecules on each facets of the Au NPs. (b)The revised interface energies of the Au NPs.(c) The facet fraction of the supported Au NPs.**

Based on DFT calculated interfacial energies, we modeled Au NPs with radius of 5 nm size, close to the experimental samples (around 25000 atoms) and under gas environment and temperature conditions. As shown in Figure 4, the ESs of Au NPs exposed to 1 bar of molecular oxygen are predicted to change upon cooling. For temperature higher than 17 °C, the ES of Au NP is found to be a perfect truncated octahedron as in the case of the experimental observations under vacuum and under the inert Ar gas. For temperature higher than 47 °C, the ES of Au NP is found to be a perfect truncated octahedron as in the case of the experimental observations under vacuum and under the inert Ar gas. This is because at high temperature, the coverage of O_2 on all Au facets is zero, as shown in Figure 5a. Thus, the surface tension correction is zero and there is no reshaping. Interestingly, when the temperature decreases, the shape of Au NPs becomes more and more round. Indeed, the adsorption coverage curves shows that at low temperature, O_2 molecules adsorb on the (110) and (100) facets but not on (111) facets (see adsorption energies given in Table S2). The coverage on (110) facet is much larger than the one on (100) facet at the same temperature due to the stronger bonding of O_2 to (110) facet. The fundamental mechanism of the reshaping is that the bonding between the O_2 and the Au NPs reduces the surface tension of the latter. This reduction is stronger on (110) facets than on (100) and (111) facets due to the stronger interaction of O_2 molecule on (110) facet. Consequently, the γ_{110}^{int} becomes lower than γ_{111}^{int} and γ_{100}^{int} (Figure 5b). The resulting increased in the fraction of the (110) facet leads to the morphology of NP being more spherical (Figure 5c). Similar rounding behavior can also be found in the previous reports about the structure reconstruction of Cu and Pt NPs in water vapor environments and during CO oxidations, respectively.[68,69] Comparing Fig 3 and Fig 4, perfect matches between theoretical modeling and experiments are achieved. This agreement provides strong evidence that the O_2 molecules are molecularly adsorbed on the Au NPs. Note that the predicted refacetting temperature is in the range from 47 °C to 17 °C which is lower than the experimental temperatures. Although we have adopted the dispersion correction in the above calculations, the DFT-GGA method

tends to underestimate energies (surface energies and adsorption energies), which is a known artifact.[70] This results in the predicted theoretical temperatures being generally lower than the experimentally measured ones. Since the dissociative adsorption of O_2 by gold cannot be disregarded in our experiment, we have also tried to interpret our experimental observations by considering the adsorption of atomic oxygen on the Au(100), Au(111) and Au(110) facets. DFT calculations show that the adsorption of atomic oxygen is quite similar on the three low-index facets (Table S4). Thus, for dissociative adsorption of O_2 by gold, no change in particle ES is expected during cooling to RT.

Concerning H_2 adsorption on gold, DFT calculations show weak exothermic adsorption energies (Table S5). The predicted ES from the MSR model shows perfect truncated octahedron that does not evolve with pressure and temperature variations as observed experimentally. The excellent agreement between experiment and modelling is a strong indication that H_2 molecules do not adsorb readily on the Au NPs. The direct adsorption of H_2 on Au edge and corners atoms has been observed in Au NPs deposited on alumina.[32] In this system, it has been shown that H_2 adsorption is limited by kinetic factors to 23 to 100 °C with no spill-over to face sites. Similarly, DFT calculations have predicted that a single low-coordinated Au atom which can belong to defective extended surfaces or nanoparticles is sufficient to dissociate H_2.[31,71] The dissociation process involves a positive energy barrier but is spontaneous on Au atoms directly bonded to four other atoms.[71] In the present work, it is highly probable that when the NPs are cooled to RT the number of low-coordinated Au sites that can bind H_2 molecules is low. Consequently, the NPs initially retain their high-temperature Wulff-Kaishev ES at all stages.

In summary, by performing GCTEM on model supported Au NPs, we have provided the first real space observations of O_2 and H_2 reactivity on nanosized gold at atmospheric pressure. By monitoring the change in particle ES upon gas exposure, we provide experimental evidence that Au NPs supported on rutile titania (110) surfaces can directly bind O_2. Equilibrium shape reconstruction of Au NPs using the multiscale structure reconstruction

modeling undertaken in conjunction with *in situ* observations of particle morphology brings fundamental atomic level insights into the absorption processes enabling the identification of the active sites at the particle surface for O_2 adsorption. Experiments and modelling show that Au(100) and (110) facets are active in O_2 adsorption but are inactive in H_2 adsorption. In the latter case, gas absorption hardly occurs on the Au NP itself. These findings constitute key elements for the rational design of more active Au nanocatalysts for both oxidation and hydrogenation catalytic reactions. Our work provides a fundamental understanding of the structure reconstruction of TiO_2-supported Au NPs under reactive media, which offers useful guidance for the experiments in the various related research fields.

Acknowledgement

J.N acknowledges funding from the French National Research Agency through the TOTEM project, Grant Number ANR-17-CE07-0031. The authors are also grateful to Région Ile-de-France for convention SESAME E1845 for the support of the JEOL JEM-ARM200F electron microscope installed at Paris Diderot University. J. M acknowledges the funding from the China Scholarship Council (File No. 201700260147) through the 2017-2019 Sino-French Cai Yuanpei Program.

Supporting Information Available

The following files are available free of charge.

- Figure S1: HAADF-STEM images for the assessment of the morphology of gold nanoparticles supported on rutile titania nanorods
- Figure S2: TEM images of gold nanoparticles in vacuum
- Figure S3: Temperature series of HAADF-STEM images of Au NPs under 133 Pa O_2

- Figure S4: Tested adsorption sites and adsorption configurations of oxygen molecule adsorbed on (a) Au(100), (b) Au(110), and (c) Au(111) surfaces.
- Figure S5. Tested adsorption sites and adsorption configurations of H_2 molecule adsorbed on (a) Au(100), (b) Au(111), and (c) Au(110) surfaces.
- Figure S6. Adsorption configurations of atomic oxygen on (a) Au(100), (b) Au(111) and (c) Au(110) surfaces
- Figure S7. Wulff construction of Au NPs under hydrogen environment at atmospheric pressure as a function of temperature from 200 °C to 17 °C.
- Table S1. The DFT calculated surface energies of the Au(100), Au(110), and Au(111) under Vacuum.
- Table S2. Adsorption energies (eV) of oxygen molecule on Au(100), (110), and (111) surfaces.
- Table S3. Adsorption energies (eV) of hydrogen molecule on Au(100), (110), and (111) surfaces.
- Table S4. Adsorption energies (eV) of atomic oxygen on Au(100), (110), and (111) surfaces.

References

(1) Hammer, B.; N, J. K. Why Gold Is the Noblest of All the Metals. *Nature* **1995**, *376*, 238–240.

(2) Cha, D. Y.; Parravano, G. Surface Reactivity of Supported Gold : Oxygen Transfer between CO and CO_2. *Journal of Catalysis* **1970**, *18*, 200–&.

(3) Sermon, P. A.; Bond, G. C.; Wells, P. B. Hydrogenation of Alkenes Over Supported Gold. *Journal of the Chemical Society-Faraday Transactions I* **1979**, *75*, 385–394.

(4) Bond, G. C.; Sermon, P. A.; Webb, G.; Buchanan, D. A.; Wells, P. B. Hydrogenation Over Supported Gold Catalysts. *Journal of the Chemical Society-chemical Communications* **1973**, 444–445.

(5) Galvagno, S.; Parravano, G. Chemical Reactivity of Supported Gold : Reduction of NO by H_2. *Journal of Catalysis* **1978**, *55*, 178–190.

(6) Haruta, M.; Kobayashi, T.; Sano, H.; Yamada, N. Novel Gold Catalysts for the Oxidation of carbon-monoxide at a Temperature Far below 0-degrees-c. *Chemistry Letters* **1987**, 405–408.

(7) Haruta, M.; Yamada, N.; Kobayashi, T.; Iijima, S. Gold Catalysts Prepared by Coprecipitation for Low-temperature Oxidation of Hydrogen and of Carbon-monoxide. *Journal of Catalysis* **1989**, *115*, 301–309.

(8) Haruta, M. When Gold Is Not Noble: Catalysis by Nanoparticles. *The Chemical Record* **2003**, *3*, 75–87.

(9) Lopez, N.; Janssens, T. V. W.; Clausen, B. S.; Xu, Y.; Mavrikakis, M.; Bligaard, T.; N, J. K. On the origin of the catalytic activity of gold nanoparticles for low-temperature CO oxidation. *Journal of Catalysis* **2004**, *223*, 232–235.

(10) Chen, M. S.; Goodman, D. W. The structure of catalytically active gold on titania. *Science* **2004**, *306*, 252–255.

(11) Hutchings, G. J. Catalysis by gold. *Catalysis Today* **2005**, *100*, 55–61.

(12) Guzman, J.; Carrettin, S.; Corma, A. Spectroscopic evidence for the supply of reactive oxygen during CO oxidation catalyzed by gold supported on nanocrystalline CeO_2. *Journal of the American Chemical Society* **2005**, *127*, 3286–3287.

(13) Wang, J. G.; Hammer, B. Role of Au_+ in supporting and activating Au7 on TiO_2(110). *Physical Review Letters* **2006**, *97*, 136107.

(14) Comotti, M.; Della Pina, C.; Matarrese, R.; Rossi, M. The catalytic activity of "Naked" gold particles. *Angewandte Chemie-international Edition* **2004**, *43*, 5812–5815.

(15) Nijhuis, T. A. R.; Visser, T.; Weckhuysen, B. M. The role of gold in gold-titania epoxidation catalysts. *Angewandte Chemie-international Edition* **2005**, *44*, 1115–1118.

(16) Hughes, M. D.; Xu, Y. J.; Jenkins, P.; McMorn, P.; Landon, P.; Enache, D. I.; Carley, A. F.; Attard, G. A.; Hutchings, G. J.; King, F.; Stitt, E. H.; Johnston, P.; Griffin, K.; Kiely, C. J. Tunable gold catalysts for selective hydrocarbon oxidation under mild conditions. *Nature* **2005**, *437*, 1132–1135.

(17) Enache, D. I.; Edwards, J. K.; Landon, P.; Solsona-Espriu, B.; Carley, A. F.; Herzing, A. A.; Watanabe, M.; Kiely, C. J.; Knight, D. W.; Hutchings, G. J. Solvent-free oxidation of primary alcohols to aldehydes using Au-Pd/TiO_2 catalysts. *Science* **2006**, *311*, 362–365.

(18) Abad, A.; Corma, A.; Garcia, H. Catalyst parameters determining activity and selectivity of supported gold nanoparticles for the aerobic oxidation of alcohols: The molecular reaction mechanism. *Chemistry-a European Journal* **2008**, *14*, 212–222.

(19) Fu, Q.; Saltsburg, H.; Flytzani-Stephanopoulos, M. Active nonmetallic Au and Pt species on ceria-based water-gas shift catalysts. *Science* **2003**, *301*, 935–938.

(20) Hutchings, G. J. Nanocrystalline gold and gold palladium alloy catalysts for chemical synthesis. *Chemical Communications* **2008**, 1148–1164.

(21) Edwards, J. K.; Solsona, B.; N, E. N.; Carley, A. F.; Herzing, A. A.; Kiely, C. J.; Hutchings, G. J. Switching Off Hydrogen Peroxide Hydrogenation in the Direct Synthesis Process. *Science* **2009**, *323*, 1037–1041.

(22) Jia, J. F.; Haraki, K.; Kondo, J. N.; Domen, K.; Tamaru, K. Selective hydrogenation of acetylene over Au/Al_2O_3 catalyst. *Journal of Physical Chemistry B* **2000**, *104*, 11153–11156.

(23) Schimpf, S.; Lucas, M.; Mohr, C.; Rodemerck, U.; Bruckner, A.; Radnik, J.; Hofmeister, H.; Claus, P. Supported gold nanoparticles: in-depth catalyst characterization and application in hydrogenation and oxidation reactions. *Catalysis Today* **2002**, *72*, PII S0920–5861(01)00479–5.

(24) Mohr, C.; Hofmeister, H.; Radnik, J.; Claus, P. Identification of active sites in gold-catalyzed hydrogenation of acrolein. *Journal of the American Chemical Society* **2003**, *125*, 1905–1911.

(25) Corma, A.; Serna, P. Chemoselective hydrogenation of nitro compounds with supported gold catalysts. *Science* **2006**, *313*, 332–334.

(26) Tsubota, S.; Nakamura, T.; Tanaka, K.; Haruta, M. Effect of calcination temperature on the catalytic activity of Au colloids mechanically mixed with TiO_2 powder for CO oxidation. *Catalysis Letters* **1998**, *56*, 131–135.

(27) Mavrikakis, M.; Stoltze, P.; Norskov, J. K. Making gold less noble. *Catalysis Letters* **2000**, *64*, 101–106.

(28) Arrii, S.; Morfin, F.; Renouprez, A. J.; Rousset, J. L. Oxidation of CO on gold supported catalysts prepared by laser vaporization: Direct evidence of support contribution. *Journal of the American Chemical Society* **2004**, *126*, 1199–1205.

(29) Zanella, R.; Giorgio, S.; Shin, C. H.; Henry, C. R.; Louis, C. Characterization and reactivity in CO oxidation of gold nanoparticles supported on TiO_2 prepared by deposition-precipitation with NaOH and urea. *Journal of Catalysis* **2004**, *222*, 357–367.

(30) Boronat, M.; Illas, F.; Corma, A. Active Sites for H_2 Adsorption and Activation in Au/TiO_2 and the Role of the Support. *Journal of Physical Chemistry A* **2009**, *113*, 3750–3757.

(31) Boronat, M.; Concepcion, P.; Corma, A. Unravelling the Nature of Gold Surface Sites by Combining IR Spectroscopy and DFT Calculations. Implications in Catalysis. *Journal of Physical Chemistry C* **2009**, *113*, 16772–16784.

(32) Bus, E.; Miller, J. T.; van Bokhoven, J. A. Hydrogen chemisorption on Al_2O_3-supported gold catalysts. *Journal of Physical Chemistry B* **2005**, *109*, 14581–14587.

(33) Fujitani, T.; Nakamura, I.; Akita, T.; Okumura, M.; Haruta, M. Hydrogen Dissociation by Gold Clusters. *Angewandte Chemie-international Edition* **2009**, *48*, 9515–9518.

(34) Luza, L.; Rambor, C. P.; Gual, A.; Fernandes, J. A.; Eberhardt, D.; Dupont, J. Revealing Hydrogenation Reaction Pathways on Naked Gold Nanoparticles. *ACS Catalysis* **2017**, *7*, 2791–2799.

(35) Mills, G.; Gordon, M. S.; Metiu, H. Oxygen adsorption on Au clusters and a rough Au(111) surface: The role of surface flatness, electron confinement, excess electrons, and band gap. *Journal of Chemical Physics* **2003**, *118*, 4198–4205.

(36) Roldan, A.; Gonzalez, S.; Ricart, J. M.; Illas, F. Critical size for O_2 dissociation by Au nanoparticles. *ChemPhysChem* **2009**, *10*, 348–351.

(37) Kotobuki, M.; Leppelt, R.; Hansgen, D. A.; Widmann, D.; Behm, R. J. Reactive oxygen on a Au/TiO_2 supported catalyst. *Journal of Catalysis* **2009**, *264*, 67–76.

(38) Boronat, M.; Corma, A. Oxygen activation on gold nanoparticles: separating the influence of particle size, particle shape and support interaction. *Dalton Transactions* **2010**, *39*, 8538–8546.

(39) Widmann, D.; Behm, R. J. Active Oxygen on a Au/TiO_2 Catalyst: Formation, Stability, and CO Oxidation Activity. *Angewandte Chemie-international Edition* **2011**, *50*, 10241–10245.

(40) Sun, K.; Kohyama, M.; Tanaka, S.; Takeda, S. Direct O_2 Activation on Gold/Metal Oxide Catalysts through a Unique Double Linear O-Au-O Structure. *CheCatChem* **2013**, *5*, 2217–2222.

(41) Tao, F. F.; Salmeron, M. In Situ Studies of Chemistry and Structure of Materials in Reactive Environments. *Science* **2011**, *331*, 171–174.

(42) Meng, J.; Zhu, B.; Gao, Y. Shape Evolution of Metal Nanoparticles in Binary Gas Environment. *Journal of Physical Chemistry C* **2018**, *122*, 6144–6150.

(43) Duan, M.; Yu, J.; Meng, J.; Zhu, B.; Wang, Y.; Gao, Y. Reconstruction of Supported Metal Nanoparticles in Reaction Conditions. *Angewandte Chemie-international Edition* **2018**, *57*, 6464–6469.

(44) Genty, E.; Jacobs, L.; de Bocarme, T. V.; Barroo, C. Dynamic Processes on Gold-Based Catalysts Followed by Environmental Microscopies. *Catalysts* **2017**, *7*, 134.

(45) Tao, F. F.; Crozier, P. A. Atomic-Scale Observations of Catalyst Structures under Reaction Conditions and during Catalysis. *Chemical Reviews* **2016**, *116*, 3487–3539.

(46) Datye, A. K. Electron microscopy of catalysts: recent achievements and future prospects. *Journal of Catalysis* **2003**, *216*, 144–154.

(47) Giorgio, S.; Joao, S. S.; Nitsche, S.; Chaudanson, D.; Sitja, G.; Henry, C. R. Environmental electron microscopy (ETEM) for catalysts with a closed E-cell with carbon windows. *Ultramicroscopy* **2006**, *106*, 503–507.

(48) Giorgio, S.; Cabie, M.; Henry, C. R. Dynamic observations of Au catalysts by environmental electron microscopy. *Gold Bulletin* **2008**, *41*, 167–173.

(49) Yang, J. C.; Small, M. W.; Grieshaber, R. V.; Nuzzo, R. G. Recent developments and applications of electron microscopy to heterogeneous catalysis. *Chemical Society Reviews* **2012**, *41*, 8179–8194.

(50) Hansen, T. W.; Wagner, J. B. Catalysts under Controlled Atmospheres in the Transmission Electron Microscope. *Acs Catalysis* **2014**, *4*, 1673–1685.

(51) Bugnet, M.; Overbury, S. H.; Wu, Z. L.; Epicier, T. Direct Visualization and Control of Atomic Mobility at 100 Surfaces of Ceria in the Environmental Transmission Electron Microscope. *Nano Letters* **2017**, *17*, 7652–7658.

(52) Dembele, K.; Moldovan, S.; Hirlimann, C.; Harmel, J.; Soulantica, K.; Serp, P.; Chaudret, B.; Gay, A. . S.; Maury, S.; Berliet, A.; Fecant, A.; Ersen, O. Reactivity and structural evolution of urchin-like Co nanostructures under controlled environments. *Journal of Microscopy* **2018**, *269*, 168–176.

(53) Uchiyama, T.; Yoshida, H.; Kuwauchi, Y.; Ichikawa, S.; Shimada, S.; Haruta, M.; Takeda, S. Systematic Morphology Changes of Gold Nanoparticles Supported on CeO_2 during CO Oxidation. *Angewandte Chemie-international Edition* **2011**, *50*, 10157–10160.

(54) Yoshida, H.; Kuwauchi, Y.; Jinschek, J. R.; Sun, K.; Tanaka, S.; Kohyama, M.; Shimada, S.; Haruta, M.; Takeda, S. Visualizing Gas Molecules Interacting with Supported Nanoparticulate Catalysts at Reaction Conditions. *Science* **2012**, *335*, 317–319.

(55) Li, H.; Afanasiev, P. On the selective growth of titania polymorphs in acidic aqueous medium. *Materials Research Bulletin* **2011**, *46*, 2506–2514.

(56) Bagheri, S.; Muhd Julkapli, N.; Bee Abd Hamid, S. Titanium dioxide as a catalyst support in heterogeneous catalysis. *The Scientific World Journal* **2014**, *2014*, 727496–727496.

(57) Diebold, U. The surface science of titanium dioxide. *Surface Science Reports* **2003**, *48*, PII S0167–5729(02)00100–0.

(58) Haruta, M.; Tsubota, S.; Kobayashi, T.; Kageyama, H.; Genet, M. J.; Delmon, B. Low-temperature Oxidation of Co Over Gold Supported on TiO_2, $\alpha - Fe_2O_2$, and Co_3O_4. *Journal of Catalysis* **1993**, *144*, 175–192.

(59) Tai Nguyen, N.; Nelayah, J.; Afanasiev, P.; Piccolo, L.; Alloyeau, D.; Ricolleau, C. Structural Properties of Catalytically Active Bimetallic Gold-Palladium Nanoparticles Synthesized on Rutile Titania Nanorods by Pulsed Laser Deposition. *Crystal Growth & Design* **2018**, *18*, 68–76.

(60) Métois, J. J.; Heyraud, J. C. Sem Studies of Equilibrium Forms - Roughening Transition and Surface Melting of Indium and Lead Crystals. *Ultramicroscopy* **1989**, *31*, 73–79.

(61) Quan, Z.; Wang, Y.; Fang, J. High-Index Faceted Noble Metal Nanocrystals. *Accounts of Chemical Research* **2013**, *46*, 191–202.

(62) Fujita, T.; Guan, P.; McKenna, K.; Lang, X.; Hirata, A.; Zhang, L.; Tokunaga, T.; Arai, S.; Yamamoto, Y.; Tanaka, N.; Ishikawa, Y.; Asao, N.; Yamamoto, Y.; Erlebacher, J.; Chen, M. Atomic origins of the high catalytic activity of nanoporous gold. *Nature Materials* **2012**, *11*, 775–780.

(63) Wulff, G. On the question of speed of growth and dissolution of crystal surfaces. *Zeitschrift Fur Krystallographie Und Mineralogie* **1901**, *34*, 449–530.

(64) Langmuir, I. The Adsorption of Gases on Plane Surfaces of Glass, Mica and Platinum. *Journal of the American Chemical Society* **1918**, *40*, 1361–1403.

(65) Zhu, B.; Xu, Z.; Wang, C.; Gao, Y. Shape Evolution of Metal Nanoparticles in Water Vapor Environment. *Nano Letters* **2016**, *16*, 2628–2632.

(66) Zhu, B.; Meng, J.; Gao, Y. Equilibrium Shape of Metal Nanoparticles under Reactive Gas Conditions. *Journal of Physical Chemistry C* **2017**, *121*, 5629–5634.

(67) `http://kinetics.nist.gov/janaf/`.

(68) Hansen, P. L.; Wagner, J. B.; Helveg, S.; Rostrup-Nielsen, J. R.; Clausen, B. S.; Topsoe, H. Atom-resolved imaging of dynamic shape changes in supported copper nanocrystals. *Science* **2002**, *295*, 2053–2055.

(69) Vendelbo, S. B.; Elkjaer, C. F.; Falsig, H.; Puspitasari, I.; Dona, P.; Mele, L.; Morana, B.; Nelissen, B. J.; van Rijn, R.; Creemer, J. F.; Kooyman, P. J.; Helveg, S. Visualization of oscillatory behaviour of Pt nanoparticles catalysing CO oxidation. *Nature Materials* **2014**, *13*, 884–890.

(70) Gautier, S.; Steinmann, S. N.; Michel, C.; Fleurat-Lessard, P.; Sautet, P. Molecular adsorption at Pt(111). How accurate are DFT functionals? *Physical Chemistry Chemical Physics* **2015**, *17*, 28921–28930.

(71) Corma, A.; Boronat, M.; Gonzalez, S.; Illas, F. On the activation of molecular hydrogen by gold: a theoretical approximation to the nature of potential active sites. *Chemical Communications* **2007**, 3371–3373.

Graphical TOC Entry

Some journals require a graphical entry for the Table of Contents. This should be laid out "print ready" so that the sizing of the text is correct.
Inside the `tocentry` environment, the font used is Helvetica 8 pt, as required by *Journal of the American Chemical Society*.
The surrounding frame is 9 cm by 3.5 cm, which is the maximum permitted for *Journal of the American Chemical Society* graphical table of content entries. The box will not resize if the content is too big: instead it will overflow the edge of the box.
This box and the associated title will always be printed on a separate page at the end of the document.